Theoretical and Applied Mechanics Letters 13 (2023) 100466

Contents lists available at ScienceDirect

Theoretical and Applied Mechanics Letters

journal homepage: www.elsevier.com/locate/taml

Review

An overview of fluids mixing in T-shaped mixers☆

Huixin Li[a], Duo Xu[a,b,*]

[a] The State Key Laboratory of Nonlinear Mechanics, Institute of Mechanics, Chinese Academy of Sciences, Beijing, 100190, China
[b] School of Engineering Science, University of Chinese Academy of Sciences, Beijing, 100049, China

ARTICLE INFO

Article history:
Received 18 May 2023
Revised 24 June 2023
Accepted 3 July 2023
Available online 11 July 2023

Keywords:
T-mixer
Mixing
Numerical simulations
Experiments

ABSTRACT

In a T-shaped mixer, the two liquid streams in the inlet channels meet each other at the T-junction, and their liquid-liquid contacting face exhibits planar, swirling folds and the folds breaking to be chaos and turbulence, as the Reynolds number increases. The characteristic mixing scenario attracts long-time attention, given these mixings are of fundamental importance in fluid physics and also have been successfully used in engineering applications. The experimental and numerical studies of flow features and mixing characteristics in T-mixers are overviewed in this manuscript. This review introduces the experimental and numerical techniques in the studies, the flow and mixing characteristics in the corresponding regimes and application examples of the T-mixers at last, aiming at introducing fundamentals to researchers with initial interests on this topic.

1. Introduction

Miscible liquid-liquid mixing is a fundamental process in engineering applications. In chemical engineering, micro-mixing devices are favored to investigate mixing processes and assess their influence on chemical reactions [1]. Among various canonical mixers, T-shaped mixers have been widely employed, given that they exhibit good mixing efficiency and enable the precise control of mixing processes for various applications. A T-mixer has two inlet branches and one outlet, and the overall shape of the mixer is in a letter *'T'*, see a sketched example in Fig. 1a. This device has been successfully applied in liquid antisolvent precipitation (LAP) method to produce nano/micro-sized drug particles to improve bioavailability of the pharmaceutical drugs. Here a liquid solvent (e.g. ethanol) which is well mixed with the drug ingredient flows into the T-mixer from one inlet, while an antisolvent liquid (e.g. water) enters the T-mixer from the other inlet. The two fluids mixes at their miscible interface, when they are advected towards the outlet. The mixing process leads to the precipitation of nano/micro-particles, and their sizes are closely associated with the mixing efficiency. When two fluids mix, their contacting interface enlarges during their interplay entrainment, and may exhibit distinct scale interactions of the flow structures when chaos/turbulence emerges. These characteristics can be seen and well demonstrated in the flow of the T-mixer. Given this, the T-mixer can be also used for better understanding of the fundamental mixing physics, the evaluation of mixing performance, and the quantification of mixing outcomes [2,3].

Pattern formation and mixing scenario are investigated in depth in T-mixers at moderate Reynolds numbers [4–10]. Flow regimes have been accordingly identified for different flow patterns characterized with steady symmetry, engulfment, unsteady symmetry and chaos (as sketched in Fig. 2), as the Reynolds number is gradually increased. At higher Reynolds numbers, featureless turbulence of the mixing can be observed [6,11].

The investigations in T-mixers have been conducted in both experiments and numerical simulations. For the former, the velocity and concentration in micrometer-scale T-mixers are measured using micro-particle image velocimetry (μPIV) and micro-laser-induced fluorescence (μLIF), respectively [12,13], while larger T-mixers in size of centimeters have been investigated using common centimeter-scale PIV and PLIF methods [4,7,14]. For the simulations, commercial software has been used for simulations at low Reynolds number [9,10,15], whereas for larger Reynolds numbers direct numerical simulation (DNS) is favored to shed light on the complex scale interactions in the mixing process [6,16,17].

☆ This document is the results of the research project funded by the National Natural Science Foundation of China.

* Corresponding author.
E-mail address: duo.xu@imech.ac.cn (D. Xu).

https://doi.org/10.1016/j.taml.2023.100466

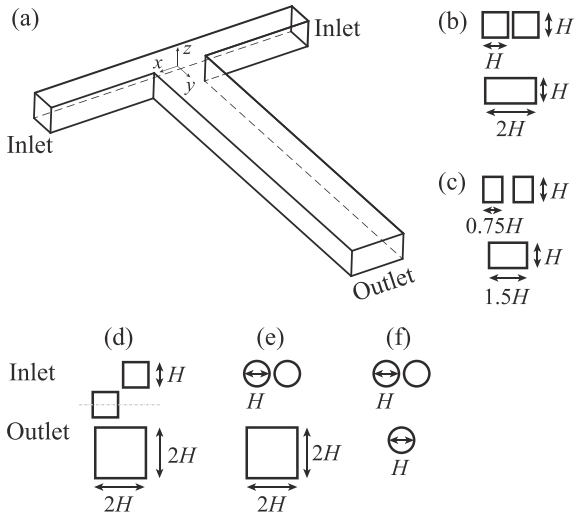

Fig. 1. (a) A schematic illustration of a T-junction section, where a Cartesian coordinate is set with the origin located at the centerpoint of the junction. (b–f) Geometries of the inlets and the outlet.

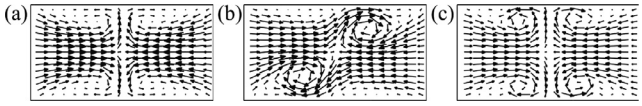

Fig. 2. Schematic illustration of the mixing patterns within the $y/H = 0$ plane of the T-mixer: (a) steady symmetric flow, (b) engulfment flow, and (c) unsteady symmetric flow.

The flow mixing and its precipitated outcomes in micro-mixers have been reviewed in Camarri et al. [2], Cai et al. [3], Thorat and Dalvi [18], while the design principle of these micro-mixing devices is reviewed in Shi et al. [19]. This manuscript provides an overview of the fluids mixing in T-mixers, with particular considerations of introducing the elementary fundamentals to researchers, who have initial interests on this topic. The following of this manuscript is structured with the governing equations (Section 2), experimental studies (Section 3) and numerical studies (Section 4). The applications of using the T-mixers in practice is then introduced (Section 5) before a summary is drawn at last (Section 6).

2. Geometry and flow governing equations

The mixers in this review are 'T'-shaped. Varieties of the inlet and outlet in dimension aspect ratio, geometry and their combination have been used in studies. Fani et al. [5] and Fani et al. [20] used rectangular inlets with width-to-height aspect ratio 0.75 and a rectangular outlet with the aspect ratio 1.5 (see Fig. 1c). Zhang et al. [21] and Chan et al. [22] used square but non-aligned tangential inlets as sketched in Fig. 1d. Schwertfirm et al. [23] used the circular inlets (with diameter H) and the square outlet (with edge $2H$), as shown in Fig. 1e. Gao et al. [24] and Chicchiero et al. [25] used circular inlets and a circular outlet with the same diameter H (see Fig. 1f), which receives less attention in studies, despite the circular pipes commonly investigated in fluid dynamics. Gao et al. [24] and Chicchiero et al. [25] found that the T-mixers with circular inlets and a circular outlet exhibit lower mixing efficiency compared to T-mixers with rectangular inlets (including square inlets) and a rectangular outlet. In contrast, T-mixers with non-aligned tangential inlets can enhance mixing efficiency by taking advantage of the vortical flow [21,26]. Among various geometric configurations, the T-mixers with rectangular inlets (including square inlets) and a rectangular outlet are preferred for their ability to maintain relatively high mixing efficiency and the simplicity in configuration to facilitate experimental and model analysis [2].

The most commonly used T-mixer is sketched in Fig. 1a and b, where both inlets have the same square shape with a height of H and the outlet is rectangular in shape with the height of H and width of $2H$. The Cartesian coordinate (x, y, z) is usually set as sketched in Fig. 1a that x is along the inlet channels and y is along the streamwise direction of the outlet channel, while the origin is set at the center of the T-junction.

The flows in a T-mixer are depicted by the dimensionless incompressible Navier-Stokes (NS) equations

$$\frac{\partial \boldsymbol{u}}{\partial t} + \boldsymbol{u} \cdot \nabla \boldsymbol{u} = -\nabla p + \frac{1}{Re}\Delta \boldsymbol{u}, \quad \nabla \cdot \boldsymbol{u} = 0, \tag{1}$$

where p is the pressure and $\boldsymbol{u} = (u, v, w)$ is the flow velocity. $Re = u_0 H/\nu$ is the Reynolds number, where u_0 is the mean velocity at the inlet and ν is the kinematic viscosity of the working fluid. The concentration of the mixed solution is governed by the advection-diffusion equation

$$\frac{\partial \phi}{\partial t} + \boldsymbol{u} \cdot \nabla \phi = \frac{1}{ReSc}\Delta \phi, \tag{2}$$

where $\phi \in [0, 1]$ is passive scalar concentration, quantifying the ratio of one liquid component in the overall. $Sc = \nu/D$ is the Schmidt number, where D is coefficient of molecular diffusion. In a liquid-liquid mixing system, with $D \sim 10^{-9}$ m^2/s and $\nu \sim 10^{-5}$ m^2/s, Sc is of the order of 10^3. Given that the studies mainly consider the liquid-liquid mixing in this system, the current studies focus on the effect of the Reynolds numbers on the flow characteristics, lacking the investigating the effects of Sc on the flows.

3. Experimental investigation for flows in T-mixers

In the experimental investigations, flow visualization, particle image velocimetry (PIV), and planar laser-induced fluorescence (PLIF) are commonly utilized to study the flow and mixing characteristics. Chemical reactions, such as the Villermaux-Dushman reaction [27], are employed to quantify the mixing efficiency. Here we focus on PIV, PLIF technologies and the chemical reactions, which are favored given that they can provide quantitative measurement results that are required for detailed comparisons.

3.1. Experimental methods: PIV and PLIF

PIV is an optical method used to measure instantaneous velocity of flows. For using PIV, the fluid is seeded with small tracers, which have negligible buoyancy and inertia. The tracers are illuminated with a powerful light source (e.g., laser), allowing them to be clearly visualized and recorded by one or multiple cameras. Assuming negligible slip between the tracers and their ambient fluid, the flow velocity approximately equals to the tracer velocity. The motion of the tracers can be determined using the cross-correlation from paired tracer images, triple images or time-series images, with advanced algorithms [28], as illustrated in Fig. 3. Most widely used method is using the cross-correlation for a pair of images, while many algorithms have been developed to improve the measurement precision (see Raffel et al. [28] for details). The cross-correlation of triple images can suppress the random correlations and improve the detectability of tracers in an interrogation window, correspondingly smaller interrogation could be used for better spatial resolution of the velocity field [29]. For the fluid trajectory correlation, the tracer pattern inside a chosen interrogation window is tracked throughout time-series images and the trajectory prediction of the tracer pattern is built with Lagrangian cross-correlation approach. It can reduce measurement error for velocity vectors compared to the results from the cross-correlation of

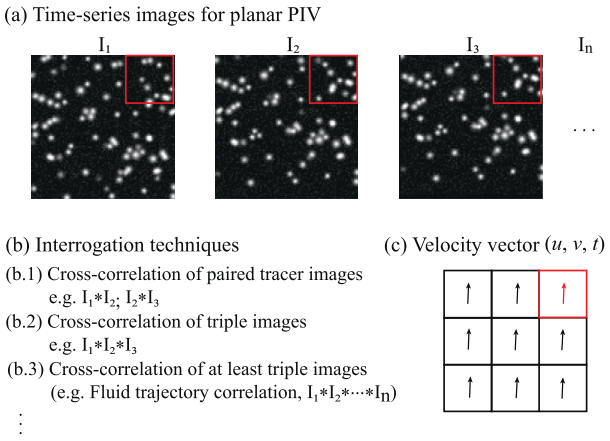

Fig. 3. (Color online) Illustration of the process of planer PIV: (a) the time series of tracer images (a portion), (b) interrogation techniques and (c) retrieved velocity vectors. Here n is the number of the captured images. The red square means a interrogation window and $*$ denotes the cross-correlation operation. (For interpretation of the references to colour in this figure legend, the reader is referred to the web version of this article.)

paired tracer images [28,30]. These advanced algorithms in PIV are available to investigate the flows in T-mixers.

In a centimeter-scale setup, the planar, stereoscopic and tomographic PIV are applicable with the two-dimensional sheet illumination or three-dimensional volumetric illumination. In the study of Thomas and Ameel [4], they used a 1mm thick laser sheet to illuminate 9 μm tracers, and implement the planar PIV to measure the 2D2C (two-dimensional two-component) flow velocities at multiple locations in the T-junction and the outlet channel of a T-mixer with $H = 20$ mm. Hoffmann et al. [12] implemented the planar μPIV in a microscope system for measuring the 2D2C flow structures in the outlet channel of a micro T-mixer. Lindken et al. [13] use the stereoscopic μPIV to measure the 2D3C velocities in a more complex setup. Their system is composed of a stereomicroscope with a filter-set for fluorescence image, a double-pulse laser and two cameras, as well as a timing unit for synchronization of the components. They use fluorescent polyethylene-glycol particles (in diameter of 572 nm) as tracers. The Self-calibration process on the tracer images was carried out to improve the quality of the tracer images before the cross-correlation operation. The 3D scan of the stereo-μPIV results of the flow are shown for the T-junction (see their Fig. 7).

PLIF is an optical technique widely used for qualitative visualization of flow structures and quantitative concentration measurements [31]. In aqueous flows, a PLIF setup consists of a light source (usually a laser) to achieve a sheet of light illumination, fluorescent dye (e.g. Rhodamine 6G) and a camera. The fluorescent dye absorbs the light illumination and spontaneously emits the fluorescent light with a wavelength shift, as shown in Fig. 4a and b. The fluorescent light signal is captured by a sensor (better with an optical lens for filtering out the illumination light). The grayscale value of the PLIF image $g(\boldsymbol{x}, t)$ has a relationship with the local dye concentration $\phi(\boldsymbol{x}, t)$ and local laser intensity $I(\boldsymbol{x}, t)$,

$$g(\boldsymbol{x}, t) = \Gamma \cdot I(\boldsymbol{x}, t) \cdot \phi(\boldsymbol{x}, t) + g_b(\boldsymbol{x}), \tag{3}$$

where Γ quantifies the system optical collection efficiency (depending on the camera sensor) as well as the effective quantum yield of fluorescence dye [31,32], and $g_b(\boldsymbol{x})$ denotes the background noise. Given that the light intensity attenuates long the light path S according to the Bouguer-Lambert-Beer Law, this leads to

$$g(\boldsymbol{x}, t) = \Gamma \cdot I_0(\boldsymbol{x}) \cdot \exp\left(-\int_S \epsilon\phi(s, t)\mathrm{d}s\right) \cdot \phi(\boldsymbol{x}, t) + g_b(\boldsymbol{x}), \tag{4}$$

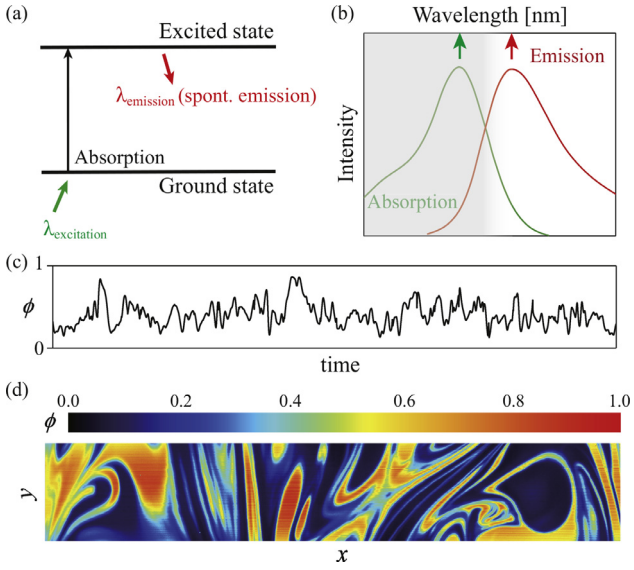

Fig. 4. (Color online) (a) The energy state of the excitation and spontaneous emission processes of the fluorescence molecular in laser-induced fluorescence (LIF). (b) The absorption and emission intensity spectrum of a fluorescence dye, and the gray (white) area represents the light blockage (pass through) by a high-pass filter. (c) An example of time-series concentration by a point LIF sensor (photo-detector). (d) A two-dimensional planar laser-induced fluorescence snapshot, adapted from Li [14]. (For interpretation of the references to colour in this figure legend, the reader is referred to the web version of this article.)

where ϵ is the attenuation coefficient of the light intensity in the working liquid. For sufficiently low dye concentration, the laser attenuation can be negligible (i.e. $\int_S \epsilon\phi(s, t)\mathrm{d}s \ll 1$), allowing the Eq. (4) to be approximately simplified to

$$g(\boldsymbol{x}, t) \approx \Gamma \cdot I_0(\boldsymbol{x}, t) \cdot \phi(\boldsymbol{x}, t) + g_b(\boldsymbol{x}). \tag{5}$$

The coefficient $\Gamma \cdot I_0(\boldsymbol{x}, t)$ can be obtained through a calibration procedure [32]. Thus, the concentration field $\phi(\boldsymbol{x}, t)$ can be obtained from the linear Eq. (5). Thomas and Ameel [4] carried out LIF measurements in a centimeter T-mixer, where the inlet is connected with a tank filled with uranine dye (a passive fluorescent dye). A continuous argon-ion laser with a wavelength of 488 nm was employed to generate a thin light sheet for exciting the dye, which emits the fluorescent light in wavelength of 512 nm. The flow structures from the LIF measurements are taken to define flow regimes. Their planar LIF measurements were assisted with point-LIF measurements, which was achieved by photodiode with illumination of laser beam via fiber optics. The planar LIF was also used in Zhang et al. [7] in a $H = 10$ mm T-mixer, where the Rhodamine 6G (with absorption wavelenght of 532 nm and emission wavelength of 560 nm) was used as the fluorescent dye. They took measurements at multiple planes of cross-section in the outlet channel. The samples of point-LIF and planar LIF measurements are shown in Fig. 4c and d, respectively.

3.2. Characterizing mixing by chemical reactions

Chemical reactions were applied to quantify the mixing scenario in T-mixers. Hessel et al. [33] used the uncolored iron ion (Fe^{3+}) and rhodanide (SCN^-) solutions, which are mixed to generate brownish complex for visualizing the flow structures. Following the similar strategy, Wong et al. [34] used the chemical reaction of the hydrolysis of dichloroacetyl phenol red (DCAPR) by sodium hydroxide (NaOH) solution to observe the mixing process. After the complete mixing of the two solutions, a dark-red color solution (appearing pink in the micro T-mixer) can be observed. The im-

age of completely hydrolysed DCAPR was used as a reference for evaluate the mixing level of flows in the T-mixer.

Another strategy to implement chemical reaction to investigate the mixing scenario relies on a set of two competing reactions, the production of which depends on the competition between the mixing effects. Falk and Commenge [27] introduced the method of extracting the intrinsic mixing time using Villermaux-Dushman reaction. This competing reaction consists of a neutralization reaction (NR) and redox reaction (RR):

$$H_2BO_3^- + H^+ \longrightarrow H_3BO_3 \qquad \text{(NR)}$$

$$5I^- + IO_3^- + 6H^+ \longleftarrow 3I_2 + 3H_2O \qquad \text{(RR)}$$

where the redox reaction (the time is in the same range of the micromixing process) is much slower than the neutralization reaction. In the T-mixer, a premix solution containing iodide I^- and iodate IO_3^- in a $H_2BO_3^-/H_3BO_3$ buffer is taken as one fluid, while another fluid containing a sulfuric acid solution that contains the protons H^+. In the case of ideal mixing, the acid is exclusively consumed by the neutralization reaction, while the redox reaction, a slower process, cannot occur due to the absence of sufficient acid. When the mixing is poor, the acid is consumed insufficiently, so that the acid can react with iodide and iodate to result the iodine I_2 (after the acid finishes the consumption of borate ions). The I_2 reacts with the iodide I^- to yield tri-iodide ions the I_3^- in a quasi-instantaneous equilibrium process:

$$I^- + I_2 \rightleftharpoons 3I_3^-. \qquad (6)$$

I_3^- can be measured by spectrophotometry. The mixing time can be then extracted from this complex process, see details in Falk and Commenge [27] and Guichardon and Falk [35]. In order to make a quantitative comparison with their simulation, Schikarski et al. [11] employed the Villermaux-Dushman reaction in a T-mixer experiment and utilized the mixing time as a measure to quantify the mixing efficiency.

3.3. Flow regimes of water-water mixing

In T-mixer experiments of passive scalar transportation and mixing in water-water system, the characteristics of the flow patterns at the plane $(x, y = 0, z)$ suddenly change as the Reynolds number is increased to across critical numbers. Accordingly, four flow regimes have been identified in experimental studies: the steady symmetric flow, the engulfment flows (including steady asymmetric flow and periodic asymmetric flow), and the unsteady symmetric flow, as well as the chaotic flows [2,4,6,21,36].

These regimes exist in the T-mixers with two squared inlets and a rectangular outlet (see Fig. 1b), a widely used configuration so that particularly focused here. When the Reynolds numbers are very low ($Re < 100$), the streams from two inlets are segregated and the mixing is only due to the molecular diffusion. As Re increases, the four-vortex flow emerges in the T-mixer, where flows are segregated around the centerline, and the molecular diffusion exclusively happens at the central interface. This vortex regime was first found in experiments by Wong et al. [34] and Thomas and Ameel [4]. They pointed out that the presence of vortices in the junction of the T-mixer has minimal effect on redistributing the concentration, when the flows remain symmetric.

For $142 < Re \leqslant 190$, it is called engulfment steady flow regime [4]. In this regime, the reflection symmetry breaks and the shear layer in the T-junction starts to engulf the two flow streams. Two vortices can be seen, and they retain a central symmetry (see Fig. 2b). In this regime, the mixing efficiency is enhanced. It can be attributed to the velocity induced by these two co-rotating vortices, which improves mixing through the advection. When $Re >$ 190, the flow steadiness cannot be sustained and the engulfment

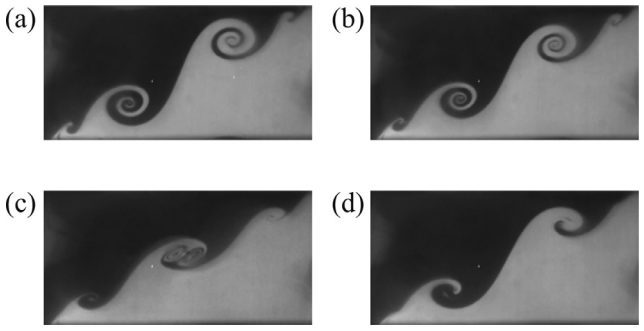

Fig. 5. PLIF images of the periodic engulfment flow pattern, every quarter of a period, at the cross-section ($y = 0$) for $Re = 237$. The figures are adapted with the permission from Zhang et al. [7] Copyright © 2019, Elsevier.

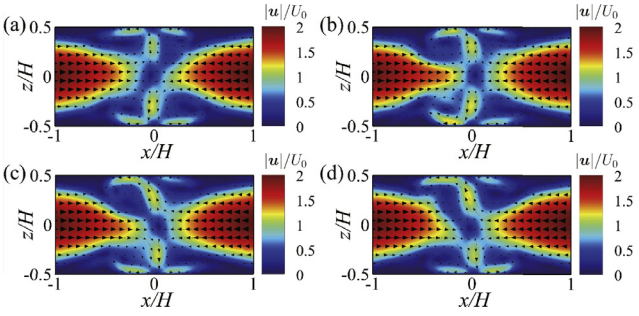

Fig. 6. (Color online) (a–d) PIV measurements of the flow velocity fields for unsteady symmetric flow at the cross-section ($y = 0$) for $Re = 360$, and the time interval between the two neighbors is a quarter of the period. The figures are reproduced from Li [14]. (For interpretation of the references to colour in this figure legend, the reader is referred to the web version of this article.)

unsteady (periodic) flow can be visualized. Here the liquid-liquid interface exhibits a periodic shear-layer process. As shown in Fig. 5, initially, two vortices gradually form at the lower left and upper right corners. Subsequently, these two vortices slowly move along with the inter-fluid interface and eventually engulf at the center of the channel, before the process repeats again.

For larger Reynolds numbers ($Re \gtrsim 320$), the flow regains the symmetry but with unsteady behavior, in the meanwhile the mixing efficiency decreases. The flow pattern exhibits the quasi-periodic behavior during the symmetric unsteady flow, where a symmetric four-vortex topology was observed (see Fig. 6). Periodic breaks from the symmetry become more frequent as Re is increased. Here the momentum field of the inlet flow in the T-mixer is more energetic [36]. As the Reynolds number is further increased, the flow regime is blended with chaos ($Re \gtrsim 400$) [9,36]. While for further larger Reynolds numbers (i.e. $Re > 500$), chaotic/turbulent flow motion was observed in simulations [6,11].

Similar flow regimes have also been observed in T-mixers with other geometric configurations. The symmetric and engulfment flow regimes have been reported in T-mixers with rectangular inlets and a rectangular outlet, which is detailed in Section 4.3. The T-mixers with non-aligned inlets, as investigated by [22] and [21], exhibit steady engulfment and unsteady engulfment flows with periodic behavior (where the flow patterns are distinct from those observed in the T-mixers with rectangular inlets and a rectangular outlet). Regarding to the T-mixers with circular inlet and outlet pipes, [25] highlight that, although the symmetric and engulfment regimes can be observed, the flow behavior significantly differs from that of T-mixers with rectangular channels. Specifically, vortices form at the curved edges of the intersection between the inlet and outlet pipes.

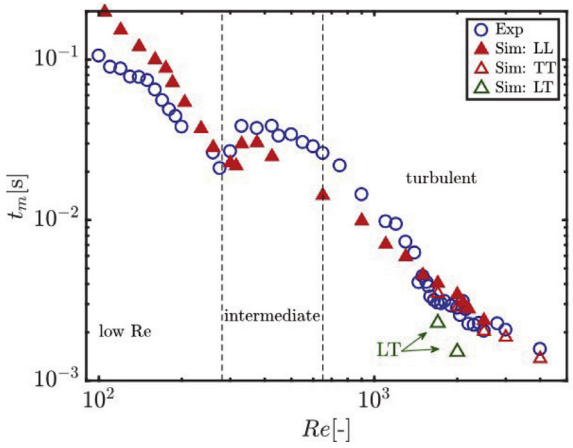

Fig. 7. (Color online) Experimentally measured mixing time t_m (circles) and computationally estimated mixing time using Eq. (11) (triangles) as a function of *Re*. Three mixing regimes are highlighted: low-*Re*, intermediate and turbulent, respectively, which is discussed in Section 4.2. ▲ and △ represent laminar-laminar (LL) and turbulent-turbulent (TT) inflow conditions, respectively. Data with laminar-turbulent (LT) inflow conditions are indicated with an arrow. The influence of the different inflow conditions is discussed in Section 4.4. Adapted with permission from Schikarski et al. [11] Copyright © 2019, Royal Society of Chemistry. (For interpretation of the references to colour in this figure legend, the reader is referred to the web version of this article.)

3.4. Mixing efficiency and mixing time

In most studies, the mixing efficiency with the intensity of segregation is quantified by

$$I_s = \frac{\sigma_b}{\sigma_{\max}}, \tag{7}$$

where $\sigma_{\max}$ is the maximum variance (determined by completely segregated streams),

$$\sigma^2_{\max} = \langle\phi\rangle(1-\langle\phi\rangle), \tag{8}$$

where

$$\langle\phi\rangle = \frac{1}{S_{\text{tot}}}\sum_{i=1}^{N} S_i\phi_i, \tag{9}$$

is the mean concentration and $S_{\text{tot}}(S_i)$ is the area of the cross section (control volume i) and N is the number of control volumes in the cross-section. The mean square deviation of the concentration

$$\sigma_b^2 = \frac{1}{S_{\text{tot}}}\int_S (\phi - \langle\phi\rangle)^2 \mathrm{d}y\mathrm{d}z = \frac{1}{S_{\text{tot}}}\sum_{i=1}^{N} S_i\left(\phi_i - \langle\phi\rangle\right)^2. \tag{10}$$

The mixing efficiency is evaluated by the local segregation at a particular point in the T-mixer, and $I_s = 1$ means completely segregated (perfectly well mixed) of the streams. In the simulation study, [11] find that the empirical relationship between the mixing time t_m and the residence time t_r (the mean residence time from the junction to the outlet of the T-mixer), i.e.

$$t_m = 1.8 I_s \cdot t_r, \tag{11}$$

renders a good agreement between the experimental and numerical measurements of the mixing time, particularly in the high *Re*-regime ($Re \gtrsim 1500$), see Fig. 7. While for low-*Re* regime, intermediate and turbulent regime, Schikarski et al. [11] concluded that the mixing time can be precisely given by the specific power input.

4. Numerical investigation for flows in T-mixer

The design of the T-mixers can be benefited from computational fluid dynamics (CFD), given that this tool allows efficient investigating the effects of geometrical configuration and operating condition on the flows.

4.1. Numerical methods and modelling

A large number of simulation investigations of flows in T-mixers are performed with commercial CFD codes, e.g. FLUENT and CFD-ACE+, based on finite volume methods. With increasing the Reynolds number, characteristic flow structures emerge with flow regimes established. However, the respective critical Reynolds numbers for the flow regimes are challenging to be precisely determined for the numerical simulations. With direct numerical simulation in FLUENT, Hussong et al. [37] systematically investigated the influence of the discretization scheme, the spatial resolution and the inlet length on the transition from flow dominated by the diffusion to the one dominated by the convection. From the tests, they concluded that the critical Reynolds number corresponding to the flow transition is lower for the upwind differencing scheme compared to the central differencing integration scheme. Zhang et al. [7] used large-eddy simulation in FLUENT equipped with Smagorinsky-Lilly subgrid model to investigate the unsteady engulfment flow, in cooperation with their own experiments. The CFD-ACE+ was applied to simulate the flows in the micro T-mixers with the finite-volume scheme [8,10], and characteristic flow patterns such as stratified flow, vortex flow and engulfment flow can be well captured for $Re \lesssim 45$, $45 \lesssim Re \lesssim 150$ and $Re \gtrsim 150$, respectively [8].

Schikarski et al. [6,11] employed a finite-volume scheme to discretize the Navier-Stokes equations in space and utilized a Runge-Kutta scheme in time, implemented using the FASTEST3D code. To ensure their simulation resolve all eddy motions, the local grid spacing $\max(\Delta x, \Delta y, \Delta z) \leqslant 2\eta_K$ was reached, where η_K is the smallest (Kolmogorov) velocity scale. They used the second-order spatial discretizations with flux limiters, which adds diffusion in space and time when large scalar gradients appear in the simulation. This numerical method is expected to be able to simulate high Reynolds number flows in the T-mixer, closer to the requirements in practice. Some studies performed direct numerical simulations of the flows in T-mixers with spectral elements method, favored by the high degree of parallelization [17,38].

4.2. Flow characteristics in water-water system

The flow regimes in the experiments of the water-water mixing are confirmed in the numerical simulations. Advanced than the experimental measurements, the simulations can provide the three-dimensional characteristic flow structures and their evolution in time.

For very low *Re*, two streams are segregated and steady vortical structures are found [8,38,39], see Fig. 8a. When *Re* is at 80–140, the flow topology becomes the four-vortex regime, as shown in Figs. 2a and 8 a. According to Kockmann et al. [10], the steady symmetric vortex pairs stem from the rapid damping of vortical structures resulted from the viscous forces. Later on, two steady three-dimensional (3D) vortical structures, like a letter 'U', are identified in simulations [5,37]. The bottom part of 'U' is formed at the confluence of the two streams, while the two legs of the counter-rotating vortical structures are in the outlet channel, see Fig. 8b. When the Reynolds number is above a critical value (usually between 138 and 155), the flow steps into engulfment steady regime, as reported in simulations [5,8,10,37–39]. In this regime, due to the loss of symmetry at the stream confluence, one leg of vortical structure is fed more fluid than the other. As a result, the two strongest legs co-rotate and persist far downstream in the outlet channel, while the two weaker legs vanish, see Fig. 8c.

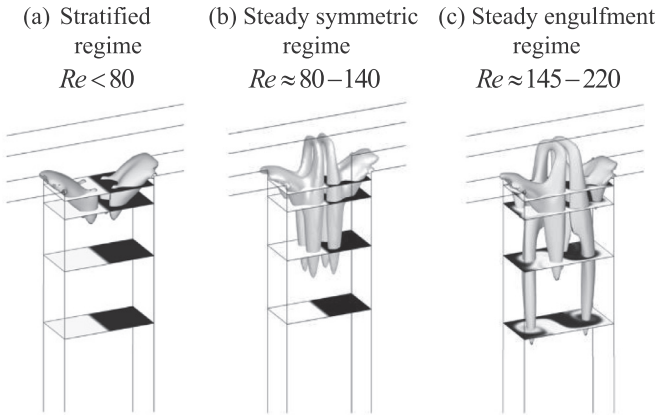

Fig. 8. The λ_2 isosurfaces of the three-dimensional vortex structures and the corresponding concentration distribution at three slices in the outlet channel: (a) stratified regime, (b) steady symmetric regime and (c) steady engulfment regime. Adapted with the permission from Mariotti et al. [38] Copyright © 2018, Elsevier.

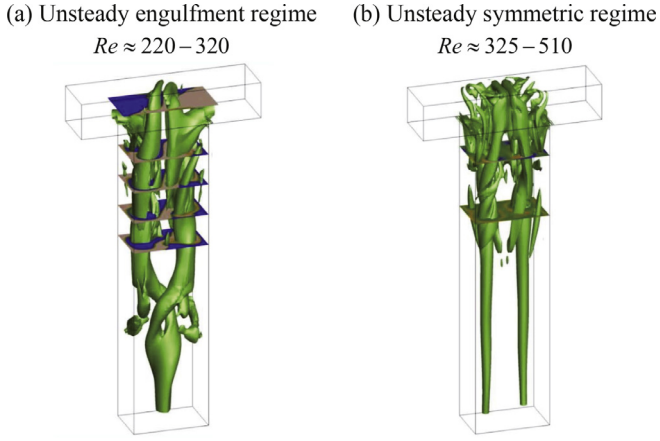

Fig. 9. (Color online) The λ_2 isosurfaces of the three-dimensional vortex structures and the corresponding concentration distribution at three slices in the outlet channel: (a) unsteady engulfment regime and (b) unsteady symmetric regime. Adapted with the permission from Fani et al. [20] Copyright © 2014, AIP Publishing. (For interpretation of the references to colour in this figure legend, the reader is referred to the web version of this article.)

For moderate *Re*, the flow is in the engulfment unsteady regime [6,15–17,20,39]. With remaining as laminar flow, periodic oscillations of the flow can be observed (e.g., Fig. 5). These periodic oscillations are found to be associated with the pulsating vortices flowing in the outlet channel [9]. The Kelvin-Helmholtz instabilities in the shear layers are believed as the origin for the formation of these pulsating vortices [9]. [20] provided a physical explanation for the periodic oscillations of the flow from the perspective of the dynamics of 3D vortical structures, which exhibit similarities to the flows in the steady engulfment regime. In the unsteady engulfment regime, the 3D vortical structures at upstream merge with the cancellation of vorticities in opposite signs, and a blob of the vorticity is generated and transported towards the channel outlet. In the meanwhile, two new structures form and replace the original structures to present the flow periodicity (Fig. 9). Here we recommend to see the video of 3D structures in [20] for better understanding of this dynamic process.

For larger *Re* ($\gtrsim 320$), studies of [6] and [38] have confirmed the presence of the unsteady symmetric regime. They found that the 3D vortical structures in this regime keep their similarity to those observed in the steady symmetric regime, for most of the time. Recently, [6] and [11] conducted a computational study on a T-shaped mixer for Reynolds numbers up to 4000, in which they ascribe the flows (at $260 \lesssim Re \lesssim 600$) as intermediate regime and the flows ($Re \gtrsim 650$) are turbulent, as shown in Fig. 7.

4.3. Effects of aspect ratio and stability analysis

Most of the T-mixers in the literature has two squared inlets and a rectangular outlet, which has an aspect ratio width/height $= 2H/H = 2$. This aspect ratio, however, may strongly affect the flow regimes and the corresponding mixing performance. The aspect ratio for the inlet channel is $\kappa_i = W_i/H$ while the aspect ratio for the outlet channel is $\kappa_o = W_o/H$. Investigations were carried out on the effect of the T-mixer configuration (i.e. κ_i and κ_o) on the determination of the Reynolds number corresponding to the transition from symmetric flows to engulfment steady flows [40–43]. Soleymani et al. [42] provided a dimensionless group of κ_i and κ_o to take into account about the aspect ratios on the transition from the vortex flow to the engulfment flow. This dimensionless group was found to be in agreement with available experimental data from various T-mixers. According to the studies conducted by Reddy Cherlo and Pushpavanam [43] and Poole et al. [40], this expression can predict the critical Reynolds number, when the height of the T-mixer is smaller than or equal to the width.

Stability analysis of the linearized Navier-Stokes equations around the baseflow were conducted for the T-mixer with aspect ratios of $\kappa_i = 0.75$ and $\kappa_o = 2\kappa_i = 1.50$ for the inlet and outlet channels, respectively [5,20]. For the T-mixer geometry considered in Fani et al. [5,20], the results showed that the onset *Re* of steady engulfment regime is about 140 and the onset of the unsteady engulfment regime is observed within the range $220 \lesssim Re_c \lesssim 230$. The effects of the aspect ratio and the stability analysis on the features and the occurrence of the regimes can be found in the review of Camarri et al. [2].

4.4. Effects of inlet flow conditions

The flow regimes in the T-mixer are identified for the fully developed Poiseuille flow achieved in the inlets. When the velocity profile deviates from the Poiseuille profile, the onset of the different regimes alters. If the flows at the T-junction are not fully de-

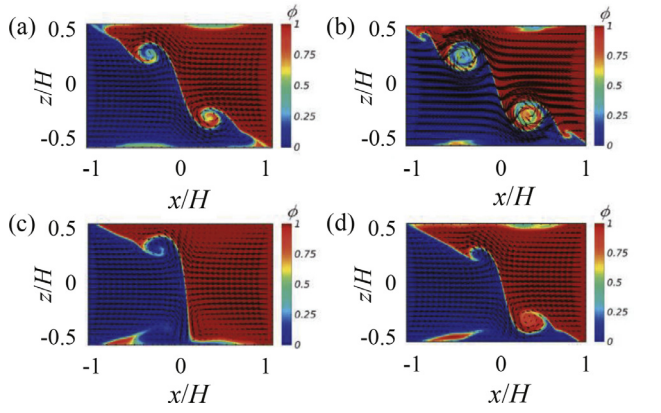

Fig. 10. (Color online) Contours of the concentration for the water-water mixing (a and b) and the water-ethanol mixing (c and d) in the engulfment regime at $Re = 160$ (a, c) and $Re = 220$ (b, d). The arrows show the cross-sectional flow velocities. The figures are adapted with permission from [6] Copyright © 2017, Elsevier. (For interpretation of the references to color in this figure legend, the reader is referred to the web version of this article.)

veloped, the engulfment flow pattern was found to occur at higher Reynolds numbers [16], and the flow exhibits significantly lower mixing efficiencies compared to the case with a fully developed flow profile. Fani et al. [5] and Fani et al. [20] also showed that for the non-fully developed case the flow tends to be more stable via the sensitivity analysis. Recently, [11] studied the influence of inlet boundary conditions (i.e., laminar-laminar, turbulent-turbulent and laminar-turbulent inflow conditions) on the efficiency of mixing at high *Re*, see Fig. 7. For instance, they reported that by utilizing mixed laminar-turbulent inflow conditions, only an approximate 1/6 specific power input is needed to reach the same mixing time (mixing efficiency) as that with the turbulent-turbulent inflow condition.

4.5. Flows and mixing in water-ethanol system

In T-mixers, few works have focused on mixtures of two different fluids, e.g., alcohol and water, a circumstance for the applications of the LAP technique. In the investigation of water-ethanol (WE) mixing, [44] observed three flow regimes (stratified, vortex, and engulfment) and found a strong correlation between mean particle size and mixing efficiency. These findings motivated Orsi et al. [45] to conduct numerical simulations of WE mixing in the steady flow regime ($Re < 200$), which confirmed the presence of flow regimes similar to those observed in water-water systems but with transitions hindered by the increased viscosity from mixing. The dependence of the viscosity on the mixture concentration was depicted in [46]. In the experiments of [44], μLIF technology is used to measure the WE mixing, but the measurement errors induced by the inhomogeneous refractive index field of the WE mixing process are not considered. This may be particularly paid attention to when using the LIF technique in larger sized T-mixers [4,7,36].

In the simulations of the water-ethanol mixing in Schikarski et al. [6], the density ρ and dynamic viscosity μ depend on the normalized concentration (mass fraction) of the water-ethanol mixture, $\phi \in [0, 1]$, see their Fig. 1b. Explicit expressions for $\rho(\phi)$ and $\mu(\phi)$ obtained from fits to the experimental data are used to accurately simulate the WE mixing for $100 < Re < 2000$. In agreement with the simulations of Schikarski et al. [6], Orsi et al. [45] reported that the transition sequence occurs at larger *Re* for WE than for water-water mixing, see Fig. 10. Further water-ethanol mixing can be found in [47] and [48].

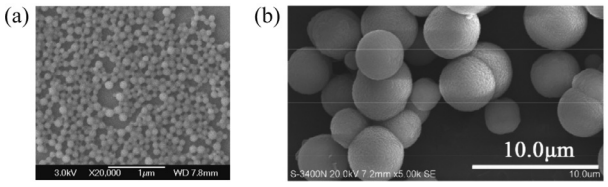

Fig. 11. (a) A typical scanning electron microscope (SEM) image of the curcumin particles by the LAP technology at $Re = 300$. The picture is adapted with permission from [44] Copyright © 2012, Elsevier. (b) The SEM image of the $MnCO_3$ microspheres with approximate sizes distributions of 2–3 μm generated by the co-precipitation method. The picture is adapted from Su et al. [49] with CC BY license (http://creativecommons.org/licenses/by/4.0/).

5. Applications

5.1. Liquid antisolvent precipitation technology

The liquid antisolvent precipitation (LAP) technology is usually applied to the nano-drugs preparation from a solution in the pharmaceutical process. In a T-mixer, a solution containing the dissolved substance is injected through one inlet and a liquid antisolvent is injected into the other inlet channel. In the junction, the mixing happens and causes the solute to precipitate out of the solution as small particles. The liquid antisolvent is typically a solvent in which the solute is not soluble, such as water for organic compounds. As studied in [44], they used the LAP technique to produce curcumin particles and a correlation between mean particle size (see Fig. 11a) and mixing efficiency was observed, that higher mixing efficiency results in smaller sized particles.

5.2. Wittig chemistry synthesis

The Wittig chemistry is a widely employed method for synthesizing vitamin A. This synthesis reaction enables the formation of a carbon bond in the production of an alkene and phosphine oxide from a phosphorane (or phosphonium ylide) and an aldehyde (or ketone). For example, a standard reactant solution (e.g., 2-nitrobenzyltriphenyl-phosphonium bromide in dry MeOH) flows into the T-mixer from one inlet and the other reactant (e.g., Methyl 4-formylbenzoate was premixed with sodium methoxide solution) was injected through the other inlet. The Wittig reaction then occurs in the junction of the T-mixer. The T-mixer can rapidly generate products in sufficient amount. This characteristic of T-mixers has significant implications for establishing high throughput chemistries, therefore presenting a promising method for future advancements in the field of chemical synthesis [50].

5.3. Co-precipitation method

The co-precipitation method is a commonly used technique for large-scale production in commercial fields. The size and distribution of particles produced by this method depend on mass transfer and dispersion in the reactor. The use of a T-mixer enables precise control of flow rates and enhances mixing effects, thereby shortening the reaction time and facilitating control over the reaction process. For instance, [49] injected two solutions of $MnSO_4{\cdot}H_2O$ and NH_4HCO_3 simultaneously into a T-mixer using an accurate syringe pump at a fixed flow rate of 50 $mL{\cdot}min^{-1}$ to produce $MnCO_3$ crystals (see Fig. 11b), which were subsequently transformed into MnO/C microspheres via calcination. The MnO/C microspheres have porous structures and an approximately uniform size. These characteristics make the MnO/C microspheres a promising anode material for Lithium-Ion batteries. The morphological and structural characteristics of these microspheres contributed to

improved electro-chemical performance of the anodes, as reported in studies of [51] and [52].

6. Summary

The T-mixer brings unique conditions to achieve mixing between two fluid streams, so that it gives successful applications in chemical and pharmaceutical engineering and can also be applied for fundamental studies of mixing physics. This manuscript presents an elementary level overview of the flow dynamics in T-mixers. With water-water mixing, steady symmetric flow, engulfment flows (including steady asymmetric flow and periodic asymmetric flow), and unsteady symmetric flow are identified in both simulations and experiments, when the Reynolds number is smaller than 500. When Reynolds numbers is above 500, chaotic and turbulent flows are observed. However, the aspect ratio and inlet conditions may give non-trivial influence on the characteristics flows and the critical Reynolds numbers corresponding to the flow regimes. In water-ethanol mixing, similar mixing scenario can be seen, but the critical Reynolds numbers for the transition among the characteristic flow patterns are delayed.

The investigations of flows in T-mixers has reached great understanding of the mixing dynamics and influence factors on mixing efficiency in numerical simulations and experiments. For the former, commercial software and self-developed codes have been used in the framework of direct numerical simulations and large eddy simulations, while the mixing of very small scales is modeled. For the latter, current experimental investigations mainly relied on 2D measurement technique, whereas 3D measurement techniques, such as Tomo-PIV, are needed for examining the 3D flow structures, which are largely reported in simulations. Current studies focus on flows and mixing for the length of the outlet channel smaller than $10H$, turbulent mixing and structures at downstream locations ($> 10H$), better approaching the fully developed flows, need further detailed investigations. Another unclear point is the effect of Schmidt number on the mixing scenarios, particularly for better understanding of the fundamental mixing physics and filling (partially) the gaps between the theory and the experiments. Overall, more efforts are necessary and greatly favored to advance the knowledge of (turbulent) mixing in T-mixers.

Declaration of Competing Interest

The authors declare that they have no known competing financial interests or personal relationships that could have appeared to influence the work reported in this paper.

Acknowledgments

This work was supported by the National Natural Science Foundation of China (Grant Nos. 11988102 and 92152106). We greatly thank Prof. Marc Avila for his tutorials and discussion on this topic.

References

[1] H.A. Stone, A.D. Stroock, A. Ajdari, Engineering flows in small devices: microfluidics toward a Lab-on-a-Chip, Annu. Rev. Fluid Mech. 36 (2004) 381–411.
[2] S. Camarri, A. Mariotti, C. Galletti, E. Brunazzi, R. Mauri, M.V. Salvetti, An overview of flow features and mixing in micro T and arrow mixers, Ind. Eng. Chem. Res. 59 (9) (2020) 3669–3686, doi:10.1021/acs.iecr.9b04922.
[3] G. Cai, L. Xue, H. Zhang, J. Lin, A review on micromixers, Micromachines (Basel) 8 (9) (2017), doi:10.3390/mi8090274.
[4] S. Thomas, T.A. Ameel, An experimental investigation of moderate Reynolds number flow in a T-channel, Exp. Fluids 49 (6) (2010) 1231–1245, doi:10.1007/s00348-010-0863-7.
[5] A. Fani, S. Camarri, M.V. Salvetti, Investigation of the steady engulfment regime in a three-dimensional T-mixer, Phys. Fluids 25 (6) (2013) 064102, doi:10.1063/1.4809591.
[6] T. Schikarski, W. Peukert, M. Avila, et al., Direct numerical simulation of water-ethanol flows in a T-mixer, Chem. Eng. J. 324 (2017) 168–181, doi:10.1016/j.cej.2017.04.119. https://linkinghub.elsevier.com/retrieve/pii/S1385894717306666
[7] J.-W. Zhang, S.-F. Liu, C. Cheng, W.-F. Li, X.-L. Xu, H.-F. Liu, F.-C. Wang, Investigation of three-dimensional flow regime and mixing characteristic in T-jet reactor, Chem. Eng. J. 358 (2019) 1561–1573, doi:10.1016/j.cej.2018.10.112. https://www.sciencedirect.com/science/article/pii/S1385894718320655
[8] M. Engler, N. Kockmann, T. Kiefer, P. Woias, Numerical and experimental investigations on liquid mixing in static micromixers, Chem. Eng. J. 101 (1) (2004) 315–322, doi:10.1016/j.cej.2003.10.017. https://www.sciencedirect.com/science/article/pii/S138589470400066X
[9] S. Dreher, N. Kockmann, P. Woias, Characterization of laminar transient flow regimes and mixing in T-shaped micromixers, Heat Transf. Eng. 30 (1–2) (2009) 91–100, doi:10.1080/01457630802293480.
[10] N. Kockmann, C. Föll, P. Woias, Flow regimes and mass transfer characteristics in static micromixers, in: H. Becker, P. Woias (Eds.), Microfluidics, BioMEMS, and Medical Microsystems, Vol. 4982, SPIE, International Society for Optics and Photonics, 2003, pp. 319–329, doi:10.1117/12.478157.
[11] T. Schikarski, H. Trzenschiok, W. Peukert, M. Avila, Inflow boundary conditions determine T-mixer efficiency, React. Chem. Eng. 4 (3) (2019) 559–568, doi:10.1039/C8RE00208H. Publisher: The Royal Society of Chemistry
[12] M. Hoffmann, M. Schlüter, N. Räbiger, Experimental investigation of liquid-liquid mixing in T-shaped micro-mixers using μ-LIF and μ-PIV, Chem. Eng. Sci. 61 (9) (2006) 2968–2976, doi:10.1016/j.ces.2005.11.029. https://www.sciencedirect.com/science/article/pii/S0009250905008833
[13] R. Lindken, J. Westerweel, B. Wieneke, Stereoscopic micro particle image velocimetry, Exp. Fluids 41 (2) (2006) 161–171, doi:10.1007/s00348-006-0154-5.
[14] H. Li, Optical measurements of mixing processes in turbulent fluid flows, University of Bremen, 2023 Ph.D. thesis.
[15] A.V. Minakov, V.Y. Rudyak, A.A. Gavrilov, A.A. Dekterev, Mixing in a T-shaped micromixer at moderate Reynolds numbers, Thermophys. Aeromech. 19 (3) (2012) 385–395, doi:10.1134/S0869864312030043.
[16] C. Galletti, M. Roudgar, E. Brunazzi, R. Mauri, Effect of inlet conditions on the engulfment pattern in a T-shaped micro-mixer, Chem. Eng. J. 185-186 (2012) 300–313, doi:10.1016/j.cej.2012.01.046. https://www.sciencedirect.com/science/article/pii/S1385894712000496
[17] C. Galletti, A. Mariotti, L. Siconolfi, R. Mauri, E. Brunazzi, Numerical investigation of flow regimes in T-shaped micromixers: benchmark between finite volume and spectral element methods, Can. J. Chem. Eng. 97 (2) (2019) 528–541, doi:10.1002/cjce.23321.
[18] A.A. Thorat, S.V. Dalvi, Liquid antisolvent precipitation and stabilization of nanoparticles of poorly water soluble drugs in aqueous suspensions: recent developments and future perspective, Chem. Eng. J. 181–182 (2012) 1–34.
[19] H. Shi, K. Nie, B. Dong, M. Long, H. Xu, Z. Liu, Recent progress of microfluidic reactors for biomedical applications, Chem. Eng. J. 361 (2019) 635–650.
[20] A. Fani, S. Camarri, M.V. Salvetti, Unsteady asymmetric engulfment regime in a T-mixer, Phys. Fluids 26 (7) (2014) 074101, doi:10.1063/1.4885451.
[21] W. Zhang, J.-W. Zhang, W.-F. Li, H.-F. Liu, F.-C. Wang, Flow regimes and mixing characteristics in non-aligned T-jets reactors, Chem. Eng. Sci. 228 (2020) 115991, doi:10.1016/j.ces.2020.115991. https://www.sciencedirect.com/science/article/pii/S0009250920305236
[22] S.T. Chan, J.T. Ault, S.J. Haward, E. Meiburg, A.Q. Shen, Coupling of vortex breakdown and stability in a swirling flow, Phys. Rev. Fluids 4 (8) (2019) 084701.
[23] F. Schwertfirm, J. Gradl, H.C. Schwarzer, W. Peukert, M. Manhart, The low Reynolds number turbulent flow and mixing in a confined impinging jet reactor, Int. J. Heat Fluid Flow 28 (6) (2007) 1429–1442, doi:10.1016/j.ijheatfluidflow.2007.04.019. https://www.sciencedirect.com/science/article/pii/S0142727X07000665
[24] Y. Gao, D.F. Zhu, Y. Han, L. Torrente-Murciano, Rational design of the inlet configuration of flow systems for enhanced mixing, J. Flow Chem. 11 (3) (2021) 589–598.
[25] C. Chicchiero, L. Siconolfi, S. Camarri, Investigation of the symmetry-breaking instability in a T-mixer with circular cross section, Phys. Fluids 32 (12) (2020) 124106.
[26] M.A. Ansari, K.-Y. Kim, K. Anwar, S.M. Kim, Vortex micro T-mixer with non-aligned inputs, Chem. Eng. J. 181-182 (2012) 846–850, doi:10.1016/j.cej.2011.11.113. https://www.sciencedirect.com/science/article/pii/S1385894711015154
[27] L. Falk, J.M. Commenge, Performance comparison of micromixers, Chem. Eng. Sci. 65 (1) (2010) 405–411, doi:10.1016/j.ces.2009.05.045. https://www.sciencedirect.com/science/article/pii/S0009250909003819
[28] M. Raffel, C.E. Willert, F. Scarano, C.J. Kähler, S.T. Wereley, J. Kompenhans, Particle Image Velocimetry: A Practical Guide, 3rd ed., Springer, 2018.
[29] J. Westerweel, G.E. Elsinga, R.J. Adrian, Particle image velocimetry for complex and turbulent flows, Annu. Rev. Fluid Mech. 45 (1) (2013) 409–436, doi:10.1146/annurev-fluid-120710-101204.
[30] K. Lynch, F. Scarano, A high-order time-accurate interrogation method for time-resolved PIV, Meas. Sci. Technol. 24 (3) (2013) 035305.
[31] J.P. Crimaldi, Planar laser induced fluorescence in aqueous flows, Exp. Fluids 44 (6) (2008) 851–863, doi:10.1007/s00348-008-0496-2.
[32] D. Xu, J. Chen, Experimental study of stratified jet by simultaneous measurements of velocity and density fields, Exp. Fluids 53 (1) (2012) 145–162, doi:10.1007/s00348-012-1275-7.
[33] V. Hessel, S. Hardt, H. Löwe, F. Schönfeld, Laminar mixing in different interdigital micromixers: I. Experimental characterization, AlChE J. 49 (3) (2003) 566–577, doi:10.1002/aic.690490304. https://onlinelibrary.wiley.com/doi/abs/10.1002/aic.690490304

[34] S.H. Wong, M.C.L. Ward, C.W. Wharton, Micro T-mixer as a rapid mixing micromixer, Sens. Actuators B 100 (3) (2004) 359–379, doi:10.1016/j.snb.2004.02.008. https://www.sciencedirect.com/science/article/pii/S0925400504000462
[35] P. Guichardon, L. Falk, Characterization of micromixing efficiency by the iodide-iodate reaction system. Part I: experimental procedure, Chem. Eng. Sci. 55 (2000) 4233.
[36] S. Thomas, T. Ameel, J. Guilkey, Mixing kinematics of moderate Reynolds number flows in a T-channel, Phys. Fluids 22 (1) (2010) 013601, doi:10.1063/1.3283063. Publisher: American Institute of Physics
[37] J. Hussong, R. Lindken, M. Pourquie, J. Westerweel, Numerical study on the flow physics of a T-shaped micro mixer, in: M. Ellero, X. Hu, J. Fröhlich, N. Adams (Eds.), IUTAM Symposium on Advances in Micro- and Nanofluidics, Springer, Netherlands, 2009, pp. 191–205, doi:10.1007/978-90-481-2626-2_15.
[38] A. Mariotti, C. Galletti, R. Mauri, M.V. Salvetti, E. Brunazzi, Steady and unsteady regimes in a T-shaped micro-mixer: synergic experimental and numerical investigation, Chem. Eng. J. 341 (2018) 414–431, doi:10.1016/j.cej.2018.01.108. https://www.sciencedirect.com/science/article/pii/S1385894718301244
[39] D. Bothe, A. Lojewski, H.-J. Warnecke, Fully resolved numerical simulation of reactive mixing in a T-shaped micromixer using parabolized species equations, Chem. Eng. Sci. 66 (24) (2011) 6424–6440, doi:10.1016/j.ces.2011.08.045. https://www.sciencedirect.com/science/article/pii/S0009250911006142
[40] R.J. Poole, M. Alfateh, A.P. Gauntlett, et al., Bifurcation in a T-channel junction: effects of aspect ratio and shear-thinning, Chem. Eng. Sci. 104 (2013) 839–848, doi:10.1016/j.ces.2013.10.006. https://www.sciencedirect.com/science/article/pii/S0009250913006908
[41] A.S. Lobasov, A.V. Minakov, V.V. Kuznetsov, V.Y. Rudyak, A.A. Shebeleva, Investigation of mixing efficiency and pressure drop in T-shaped micromixers, Chem. Eng. Process. - Process Intensif. 134 (2018) 105–114, doi:10.1016/j.cep.2018.10.012. https://www.sciencedirect.com/science/article/pii/S0255270118310560
[42] A. Soleymani, H. Yousefi, I. Turunen, Dimensionless number for identification of flow patterns inside a T-micromixer, Chem. Eng. Sci. 63 (21) (2008) 5291–5297, doi:10.1016/j.ces.2008.07.002. https://www.sciencedirect.com/science/article/pii/S0009250908003667
[43] S.K. Reddy Cherlo, S. Pushpavanam, et al., Effect of depth on onset of engulfment in rectangular micro-channels, Chem. Eng. Sci. 65 (24) (2010) 6486–6490, doi:10.1016/j.ces.2010.08.025. https://www.sciencedirect.com/science/article/pii/S0009250910004926
[44] W. Wang, S. Zhao, T. Shao, Y. Jin, Y. Cheng, Visualization of micro-scale mixing in miscible liquids using μ-LIF technique and drug nanoparticle preparation in T-shaped micro-channels, Chem. Eng. J. 192 (2012) 252–261, doi:10.1016/j.cej.2012.03.073. https://www.sciencedirect.com/science/article/pii/S1385894712004330
[45] G. Orsi, M. Roudgar, E. Brunazzi, C. Galletti, R. Mauri, Water-ethanol mixing in T-shaped microdevices, Chem. Eng. Sci. 95 (2013) 174–183, doi:10.1016/j.ces.2013.03.015. https://www.sciencedirect.com/science/article/pii/S0009250913001887
[46] M. Dizechi, E. Marschall, Viscosity of some binary and ternary liquid mixtures, J. Chem. Eng. Data 27 (3) (1982) 358–363.
[47] C. Galletti, G. Arcolini, E. Brunazzi, R. Mauri, Mixing of binary fluids with composition-dependent viscosity in a T-shaped micro-device, Chem. Eng. Sci. 123 (2015) 300–310, doi:10.1016/j.ces.2014.11.025. https://www.sciencedirect.com/science/article/pii/S0009250914006770
[48] C. Galletti, E. Brunazzi, R. Mauri, Unsteady mixing of binary liquid mixtures with composition-dependent viscosity, Chem. Eng. Sci. 164 (2017) 333–343, doi:10.1016/j.ces.2017.02.035. https://www.sciencedirect.com/science/article/pii/S0009250917301422
[49] J. Su, H. Liang, X.-N. Gong, X.-Y. Lv, Y.-F. Long, Y.-X. Wen, Fast preparation of porous MnO/C microspheres as anode materials for Lithium-Ion batteries, Nanomaterials 7 (6) (2017) 121, doi:10.3390/nano7060121.
[50] V. Skelton, G.M. Greenway, S.J. Haswell, P. Styring, D.O. Morgan, B. Warrington, S.Y.F. Wong, The preparation of a series of nitrostilbene ester compounds using micro reactor technology, Analyst 126 (1) (2001) 7–10, doi:10.1039/B006728H. Publisher: The Royal Society of Chemistry
[51] S. Li, J. Xu, Y. Wang, G. Luo, Controllable preparation of nanoparticles by drops and plugs flow in a microchannel device, Langmuir 24 (8) (2008) 4194–4199, doi:10.1021/la800107d.
[52] Y. Liang, G. Chu, J. Wang, Y. Huang, J. Chen, B. Sun, L. Shao, Controllable preparation of nano-$CaCO_3$ in a microporous tube-in-tube microchannel reactor, Chem. Eng. Process. 79 (2014) 34–39, doi:10.1016/j.cep.2014.03.006. https://www.sciencedirect.com/science/article/pii/S0255270114000488